

PointRWKV: Efficient RWKV-Like Model for Hierarchical Point Cloud Learning

Qingdong He^{1*} Jiangning Zhang^{1*} Jinlong Peng¹ Haoyang He²
 Xiangtai Li³ Yabiao Wang¹ Chengjie Wang¹

¹Youtu Lab, Tencent ²Zhejiang University ³Nanyang Technological University

Abstract

Transformers have revolutionized the point cloud learning task, but the quadratic complexity hinders its extension to long sequences. This puts a burden on limited computational resources. The recent advent of RWKV, a fresh breed of deep sequence models, has shown immense potential for sequence modeling in NLP tasks. In this work, we present PointRWKV, a new model of linear complexity derived from the RWKV model in the NLP field with the necessary adaptation for 3D point cloud learning tasks. Specifically, taking the embedded point patches as input, we first propose to explore the global processing capabilities within PointRWKV blocks using modified multi-headed matrix-valued states and a dynamic attention recurrence mechanism. To extract local geometric features simultaneously, we design a parallel branch to encode the point cloud efficiently in a fixed radius near-neighbors graph with a graph stabilizer. Furthermore, we design PointRWKV as a multi-scale framework for hierarchical feature learning of 3D point clouds, facilitating various downstream tasks. Extensive experiments on different point cloud learning tasks show our proposed PointRWKV outperforms the transformer- and mamba-based counterparts, while significantly saving about 42% FLOPs, demonstrating the potential option for constructing foundational 3D models. Project page: <https://hithqd.github.io/projects/PointRWKV/>.

1. Introduction

Point cloud analysis is a fundamental vision task that has a wide range of applications, including autonomous driving [33], virtual reality [38], and robotics [48], etc. Unlike 2D images, the intrinsic irregularity and sparsity of point clouds make it a challenging task to conduct point cloud representation learning. Balancing accuracy and complexity simultaneously remains an enduring problem.

*Equal contributions.

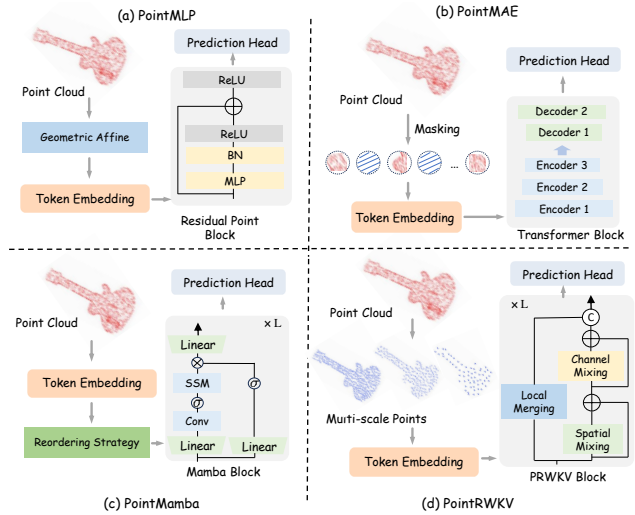


Figure 1. Architecture comparison with different methods: (a) MLP-based PointMLP [31], (b) transformer-based PointMAE [36], (c) mamba-based PointMamba [25] and (d) ours PointRWKV with linear complexity is capable of integrating the advantages of both global and local modeling, and multi-scale features endow it with more refined prediction accuracy.

Pioneered by PointNet [42] and PointNet++ [43], a series of works [3, 22, 24, 31, 45, 50, 54, 56] have emerged to follow the MLP architecture to extract geometric features (Figure 1 (a)). Recently, transformers [9, 29] have surfaced as a promising approach for point cloud analysis, demonstrating significant potential with a key component of the attention mechanism to effectively capture the relationships among a set of points. Focusing on enhancing transformers for point clouds, Point Transformers [57, 58, 69] apply vector attention and enhance the performance and efficiency for different tasks. Further, by extending self-supervised learning mechanism, some works [36, 44, 64, 66] have obtained decent performance. Among them, PointMAE [36], as depicted in Figure 1 (b), introduces a standard Transformer architecture and a shift-

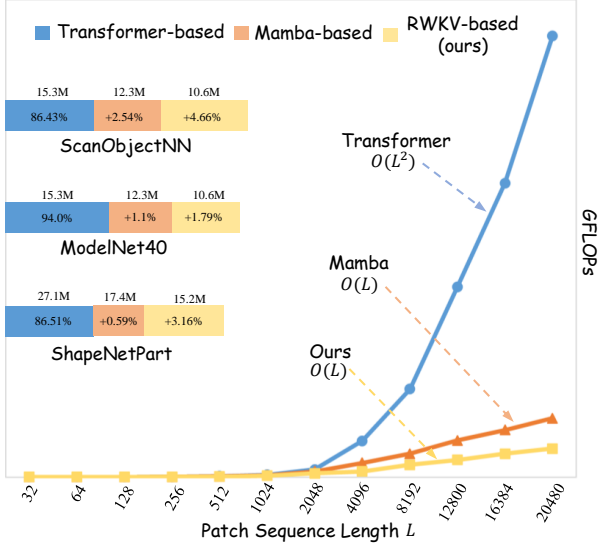


Figure 2. Accuracy-speed tradeoff. (Left) Overall accuracy acquired by different methods with relative parameters, (Right) FLOPs increase with sequence length.

ing mask tokens operation at a high ratio to reach better accuracy. However, directly applying exhaustive attention mechanisms to extended point tokens increases the demand for computational resources. This is because of the quadratic complexity inherent in attention computations, impacting both computation and memory. Furthermore, the recent state space models (SSMs) [12, 28, 70] introduce an alternative approach for point sequence modeling. Based on the structured SSMs, several works [15, 25, 26, 67] have attempted to enable the model to causally capture the point cloud structure with consistent traverse serialization mechanism or reordering strategy, as illustrated in Figure 1 (c). Albeit effective, the inherent property of unidirectional modeling of the vanilla SSM hinders them from achieving superior performance for the unordered point cloud data. Considering this, one essential question arises: *How to design a method that runs with linear complexity and achieves a high performance simultaneously?*

We notice the recent advance of RWKV [39] model within natural language processing (NLP), serving as a promising solution for attaining enhanced efficiency and handling extensive textual data. This paper pioneers the application of RWKV into the 3D point cloud learning domain, introducing PointRWKV, as illustrated in Figure 1 (d). PointRWKV maintains the core structure and benefits of RWKV while preserving the linear complexity and processing multi-scale point input. Significantly, it exhibits a reduced parameter count and computational requirement, rendering it aptly suitable for deep point cloud learning.

Specifically, PointRWKV utilizes RWKV-like architecture to model the global features of point clouds with a

series of stacked PRWKV blocks. Considering the unique properties of the strong geometric and semantic dependence between local parts and the overall 3D shapes of point cloud data, we modify the architecture into multi-stage hierarchies for progressively encoding multi-scale features of point clouds akin to an asymmetric U-Net [47]. Within each PRWKV block, we devise a parallel strategy for hierarchical point cloud feature representation, enabling local and global feature aggregation. For the original RWKV branch, we present the bidirectional quadratic expansion function with multi-headed matrix-valued states and adapt the original causal attention mechanism into a dynamic bidirectional global attention mechanism. The former can broaden the semantic scope of individual tokens, while the latter facilitates the computation of global attention within linear computation complexity. For another branch, the graph stabilizer mechanism is proposed to conduct local graph-based merging for learning the compact representation of the point cloud. These designs boost the model’s capacity while maintaining scalability and stability. In this way, our PointRWKV inherits the efficiency of RWKV in processing global information and sparse inputs while also being capable of modeling the local concept of point clouds.

By employing multi-scale pre-training, our PointRWKV can encode point clouds from local-to-global hierarchies, learning robust 3D representations and demonstrating exceptional transfer capabilities. We conduct extensive experiments on various point cloud learning tasks (*e.g.*, classification, part segmentation, and few-shot learning) to demonstrate the effectiveness of our method. As shown in Figure 2, after self-supervised pre-training on ShapeNet [5], PointRWKV achieves 93.63% (+4.66%) overall accuracy on the ScanObjectNN [51] and 96.89% (+1.79%) accuracy on ModelNet40 [59] for shape classification, 90.26% (+3.16%) instance mIoU on ShapeNetPart [62] for part segmentation, setting new state-of-the-art (SoTA) among pre-trained models. Meanwhile, PointRWKV reduces 13% in parameters and 42% in FLOPs compared to the transformer- and mamba-based counterparts, demonstrating the potential of RWKV in the 3D vision tasks. Our contributions are summarized as follows:

- We propose PointRWKV, which innovatively applies the RWKV framework to address point cloud learning tasks. This approach reaches a better balance among the parameters, computation complexity, and efficiency, making it an alternative for 3D vision tasks.
- To learn the hierarchical representations of point clouds, we introduce the multi-stage hierarchies architecture to encode multi-scale point features. Within each block in this architecture, we design the parallel strategy for hierarchical local and global feature aggregation, equipped with the bidirectional quadratic expansion, the dynamic bidirectional global attention mechanism, and the graph

stabilizer mechanism.

- Our PointRWKV exhibits state-of-the-art performance on various downstream tasks, outperforming transformer- and mamba-based counterparts in both efficiency and computation complexity, which indicates our approach to be a powerful representation learner for 3D point clouds.

2. Related Work

MLP/CNN-based Models For Point Cloud. With the progressive evolution of deep neural networks, point cloud learning has gained increasing interest, leading to the emergence of numerous deep architectures and models in recent years [7, 19–21, 31, 42]. PointNet [42] and PointNet++ [43] are the two pioneering approaches that use MLPs directly to process point clouds. Following these, a series of works [3, 6, 7, 22, 24, 31, 45, 50, 56, 68] attempt to design various deep architectures to better capture local and global geometric features. Meanwhile, several works [18, 23, 54] explore to utilize graph neural networks to construct the 3D geometric relationships between the points.

Transformer-based Models For Point Cloud. Equipped with attention mechanism, transformer [52] has evolved not only in NLP [8, 46] but also in 2D [9, 29] and 3D vision [16, 32, 35], including the point cloud learning [13, 37, 63, 69]. The Point Transformer series [57, 58, 69] are pioneering in introducing self-attention layers specifically tailored for point clouds. Significant advancements are marked by the implementation of grouped vector attention and partition-based pooling techniques for enhanced point cloud analysis. Recently, a surge of research [36, 64, 66] efforts have been directed towards enhancing point cloud data representation through self-supervised learning, particularly by leveraging masked point modeling. This self-supervised approach enables models to learn the intrinsic structure and features of point clouds in the absence of explicit labels, fostering a novel paradigm in the field.

Mamba-based Models. The Mamba model, a deep learning architecture grounded in state-space models (SSMs) [11, 12, 34, 49], exhibits enhanced processing speed and scalability by enabling selective memory retention or discarding of inputs. In recent studies, the Mamba model has demonstrated its efficacy across a diverse range of applications, such as NLP [1, 41], 2D image analysis [17, 28], and video processing [60, 60], showcasing its versatility and adaptability. Recent researches [15, 25, 26, 67] have successfully employed the Mamba model in 3D point cloud tasks, where point cloud data is represented as state vectors, allowing the model to capture the dynamic characteristics of the data, resulting in a commendable performance.

Receptance Weighted Key Value (RWKV) Models. Transformer’s memory and computational complexity scale quadratically with sequence length, while RNNs exhibit lin-

ear growth in these requirements, albeit limited by parallelization and scalability. Recently, the innovative Receptance Weighted Key Value (RWKV) [39, 40] model is introduced, seamlessly combining Transformer’s efficient parallel training with RNN’s efficient inference. Empirical results demonstrate that RWKV exhibits linear time complexity and holds promise for outperforming Transformers in long-sequence reasoning tasks. Vision-RWKV [10] is an advanced adaptation of the RWKV mechanism tailored for visual tasks, leveraging its linear computational complexity to deliver exceptional efficiency in processing high-resolution images. The following works [61, 65] also explore RWKV on dense prediction tasks. In this paper, we develop RWKV to exploit its modeling capacity and linear computational efficiency for multi-class unsupervised, making it an attractive solution for 3D point cloud learning applications.

3. Method

The overall pipeline of PointRWKV is shown in Figure 3(a), where we encode the point cloud by a hierarchical network architecture. Given an input point cloud, we first employ the multi-scale masking strategy [66] to sample different point numbers at various scales. Then a lightweight PointNet [42] is applied to embed point patches and generate token embeddings. These point tokens are consumed by the block-stacked encoder, namely the PRWKV block, where each block consists of two parallel branches for hierarchical local and global feature aggregation.

3.1. Hierarchical Point Cloud Learning

Taking an input point cloud $\mathbf{P} \in \mathbb{R}^{N \times 3}$, we apply the multi-scale masking to obtain the M scales point clouds. Starting with the point cloud as the initial M -th scale, the process involves iterative downsampling and grouping using Furthest Point Sampling (FPS) and k Nearest-Neighbour (k -NN). This results in a series of scales, each with a decreasing number of points. Then, a significant proportion of seed points at the final scale are randomly masked, leaving a subset of visible points. These visible points are then back-projected across all scales to ensure consistency. This involves retrieving the k nearest neighbors from the subsequent scale’s indices to serve as the visible positions for the current scale, with the remaining positions masked. The process yields visible and masked positions for all scales, providing a comprehensive multi-scale representation of the original point cloud. Finally, we employ a mini-PointNet to extract features for each local patch of different scales and add the positional encoding to get the final sequence, serving as the initial token embeddings $\mathbf{E}_0 \in \mathbb{R}^{T \times C}$.

PRWKV Block. After obtaining the token embeddings, we feed them into the encoder, containing a series of PRWKV blocks with long skip connections between shallow and

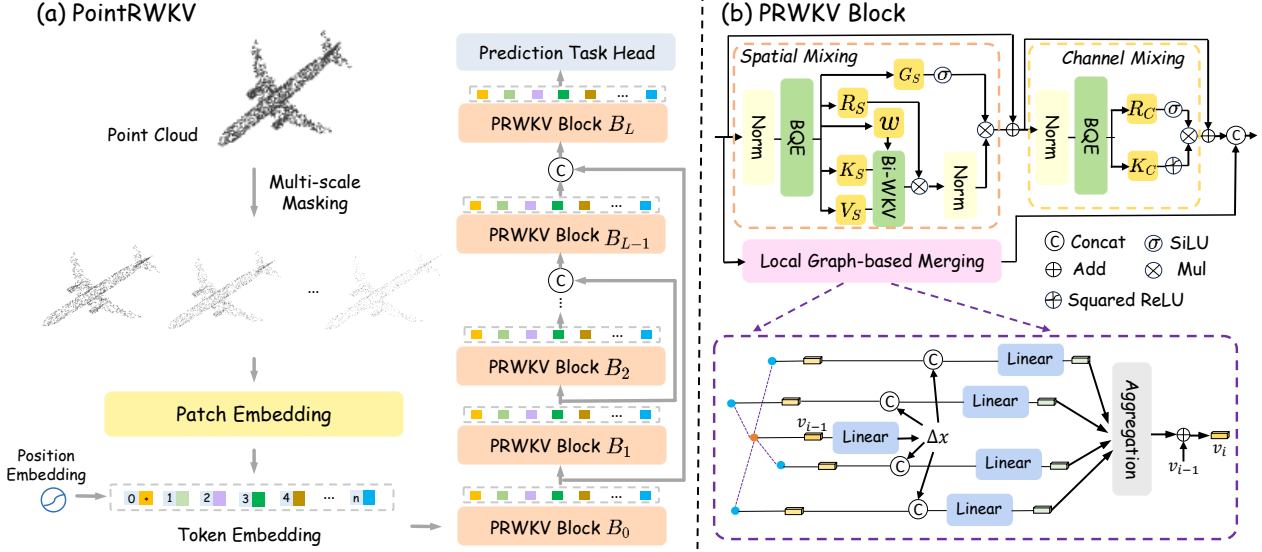


Figure 3. Overview of the proposed PointRWKV, which employs a hierarchical architecture to encode multi-scale point cloud features. The whole framework is composed of a series of PRWKV blocks which include the integrative feature modulation branch and the local graph-based merging branch to form the parallel feature learning strategy.

deep layers. Specifically, for each PRWKV block, as shown in 3(b), the two parallel branches processing strategy is employed to aggregate local and global features. The upper is the *integrative feature modulation (IFM)* flow with spatial-mixing and channel-mixing, and the below is the *local graph-based merging (LGM)*. Finally, the concatenation of the two branches is used as the output of each block.

3.2. Integrative Feature Modulation (IFM)

The integrative feature modulation branch consists of a spatial-mixing module and a channel-mixing module. The spatial-mixing module operates as an attention mechanism, executing global attention computations of linear complexity, whereas the channel-mixing module functions as a feed-forward network (FFN), facilitating feature fusion along the channel dimension.

Spatial-Mixing. After one pre-LayerNorm, the tokens are first shifted by the bidirectional quadratic expansion (BQE) function and then fed into four parallel linear layers to obtain the multi-headed vectors R_S, K_S, V_S, G_S :

$$\square_S = BQE_{\square}(X) \mathbf{W}_{\square}^S, \square \in \{R, K, V, G\}, \quad (1)$$

where BQE is formulated as :

$$\begin{aligned} BQE_{\mathcal{U}}(X) &= X + (1 - \mu_{\mathcal{U}}) X^* \\ X^* &= \text{Concat}(X_1, X_2, X_3, X_4), \end{aligned} \quad (2)$$

where $\mathcal{U} \in \{R, K, V, G, w\}$, $\mu_{\mathcal{U}}$ is the learnable vector and the X^* is the slicing vector of X , i.e., $X_1 = [b-1, n, 0 : C/4]$, $X_2 = [b+1, n, C/4 : C/2]$, $X_3 = [b, n-1, C/2 :$

$3C/4]$, $X_4 = [b, n+1, 3C/4 : C]$, b and n are the dimension index of X . The BQE function empowers the attention mechanism to inherently focus on proximate tokens across diverse channels without requiring a considerable increment in FLOPs. This procedure also broadens the receptive field of each token, thereby significantly boosting the token's coverage in the ensuing layers. Further, a new time-varying decay w is calculated by:

$$\begin{aligned} \nu(c) &= \lambda_x + \tanh(c \mathbf{A}_x) \mathbf{B}_x \\ w_{BQE}(X) &= X + (1 - \nu(BQE_w(X))) X^* \\ d &= \nu(w_{BQE}(X)) \\ w &= \exp(-\exp(d)), \end{aligned} \quad (3)$$

where λ_x is a trainable vector and $\mathbf{A}_x, \mathbf{B}_x$ are both trainable weight matrices.

Then, K_S and V_S are passed to calculate the global attention result wkv with the new decay w . Here, we introduce the linear complexity bidirectional attention mechanism with two modifications: (1) the decay parameter varies independently, which is data-dependent in a dynamic manner, and (2) the upper limit of original RWKV attention is extended from the current token t to the last token $T-1$ in the summation formula to ensure that all tokens are mutually visible in the calculation of each result. For the t -th token, the attention result is calculated by the following for-

mula:

$$wkv_t = \text{diag}(u_1, \dots, u_n) \cdot K_{S,t}^\top \cdot V_{S,t} + \sum_{i=1}^{T-1} \text{diag}(\varpi_{i,j}^1, \dots, \varpi_{i,j}^n) \cdot K_{S,i} \cdot V_{S,i} \quad (4)$$

where u is a per-channel learned boost and $\varpi_{i,j} = \prod_{j=1}^{i-1} w_j$ is a dynamic decay. The final probability output O_S is :

$$O_S = \text{Concat}(\sigma(G_S) \otimes \text{LayerNorm}(R_S \otimes wkv)) \mathbf{W}_O^S \quad (5)$$

where σ is the SiLU activation function and \otimes is the element-wise multiplication.

Channel-Mixing. The tokens from the spatial-mixing module are further passed into the channel-mixing module. Similarly, the pre-LayerNorm is utilized and R_C , K_C are obtained after the BQE operation:

$$\cap_C = \text{BQE}_{\cap}(X) \mathbf{W}_{\cap}^C, \cap \in \{R, K\}. \quad (6)$$

Afterward, a linear projection and a gate mechanism are performed, respectively. And the final output O_C is formulated as:

$$O_C = (\sigma(R_C) \otimes \text{SquaredReLU}(K_C)) \mathbf{W}_{\cap}^C \mathbf{W}_O^C. \quad (7)$$

3.3. Local Graph-based Merging (LGM)

Local geometric features have been proven to be crucial for point cloud feature learning, but RWKV’s global receptive field cannot comprehensively capture local point geometry, limiting its ability to learn fine-grained features. We encode the point cloud directly into a graph, using the points as the vertices of the graph. The edges of the graph connect neighboring points that fall within a set radius, enabling the transfer of feature information between these points. This graph representation can adapt to the structure of a point cloud without the necessity to regularize it. Furthermore, to minimize the translation variance in the local graph, we incorporate a graph stabilizer mechanism. This mechanism permits points to align their coordinates based on their unique features, improving the overall effectiveness of the network.

Graph Construction. Given the point cloud $\mathbf{P} = (p_1, p_2, \dots, p_N)$, we construct a graph $\mathbf{G} = (\mathbf{P}, \mathbf{E})$ by using \mathbf{P} as the vertices and connecting a point to its neighbors within a fixed radius r using the well-known fixed radius near-neighbors search algorithm [4], where $\mathbf{E} = \{(p_i, p_j) \mid \|x_i - x_j\|_2 < r\}$. Notably, given a cut-off distance, we utilize a cell list to find point pairs with a runtime complexity of $O(cN)$ where c is the max number of neighbors within the radius, which means this process will not increase much computation complexity.

Graph Stabilizer Mechanism. Typically, we can refine the vertex features by aggregating features along the edges within a graph neural network. In our scenario, we aim to

include a vertex’s local information about the object where the vertex belongs. So in the $(t + 1)$ -th iteration, we use the relative coordinates of the neighbors for the edge feature extraction, which can be denoted as:

$$v_i^{t+1} = g^t(\varrho(f^t(x_j - x_i, v_j^t) \mid (i, j) \in \mathbf{E}), v_i^t), \quad (8)$$

where v^t is the vertex feature from the t -th iteration, $f^t(\cdot)$ computes the edge feature between two vertices, $g^t(\cdot)$ updates the vertex features, and $\varrho(\cdot)$ is a set function that is used to accumulate the edge features for each vertex.

Despite its effectiveness, it remains susceptible to translation within the local vicinity. A slight translation added to a vertex does not significantly alter the local structure of its neighboring vertices. However, it modifies the relative coordinates of these neighbors, thereby escalating the input variance to function $f^t(\cdot)$. To diminish this translation variance, we propose the alignment of neighboring coordinates based on their structural features rather than relying on the central vertex coordinates. Since the central vertex already contains some structural features from the previous iteration, it can be used to estimate an alignment offset, prompting us to design a graph stabilizer mechanism. The Equation 8 can be rewritten as:

$$\Delta x_i^t = h^t(v_i^t) \\ v_i^{t+1} = g^t(\varrho(f^t(x_j - x_i + \Delta x_i^t, v_j^t) \mid (i, j) \in \mathbf{E}), v_i^t), \quad (9)$$

where $h^t(\cdot)$ calculates the offset using the center vertex feature value from the last iteration and Δx_i^t is the coordination offset for the vertices to stabilize their coordinates. As shown in Figure 3(b), we model $f^t(\cdot)$, $g^t(\cdot)$ and $h^t(\cdot)$ by multi-layer perception (MLP) and add a residual connection in $g^t(\cdot)$.

4. Experiments

To validate the effectiveness of our proposed PointRWKV, we conduct the following experiments: a) pre-training our model on ShapeNet [5] training set, b) evaluating our pre-trained model on various downstream tasks, including 3D object classification, 3D part segmentation, and few-shot learning, c) ablating on various strategies. Furthermore, we also conduct the experiments that training from scratch. These results can be found in the **supplementary material**.

4.1. Implementation Details

Following Point-MAE [36], we utilized the ShapeNet [5] dataset for pre-training. The configurations include using the AdamW optimizer [30] with a learning rate of 1e-3, a weight decay of 5e-2, and a cosine learning rate scheduler. The training consists of 300 epochs with a warm-up period of 10 epochs, using a batch size of 128. The model architecture comprises 12 encoder layers and 4 decoder layers.

Method	ScanObjectNN			ModelNet40		Params(M) ↓	FLOPs(G) ↓
	OBJ-BG ↑	OBJ-ONLY ↑	PB-T50-RS ↑	OA (%) ↑	mAcc (%) ↑		
<i>MLP/CNN-based</i>							
PointNet [42]	73.3	79.2	68.0	89.2	86.2	3.5	0.5
PointNet++ [43]	82.3	84.3	77.9	90.7	-	1.5	1.7
PointCNN [24]	86.1	85.5	78.5	92.2	88.1	0.6	0.9
DGCNN [54]	82.8	86.2	78.1	92.9	-	1.8	2.4
MVTN [14]	92.6	92.3	82.8	93.8	-	11.2	43.7
PointMLP [31]	-	-	85.4±0.3	94.5	91.4	12.6	31.4
PointNeXt [45]	-	-	87.7±0.4	93.2±0.1	90.8±0.2	1.4	1.6
<i>Transformer-based</i>							
Transformer [52]	79.86	80.55	77.24	91.4	-	22.1	4.8
PointTransformer [69]	-	-	-	93.7	90.6	22.1	4.8
Point-BERT [64]	87.43	88.12	83.07	93.2	-	22.1	4.8
Point-MAE [36]	90.02	88.29	85.18	93.8	-	22.1	4.8
Point-M2AE [66]	91.22	88.81	86.43	94.0	-	15.3	3.6
<i>Mamba-based</i>							
PCM [67]	-	-	88.10±0.3	93.4±0.2	-	34.2	45.0
PointMamba [25]	90.71	88.47	84.87	93.6	-	12.3	3.6
Mamba3D [15]	95.18	92.60	88.97	95.1	-	16.9	3.9
<i>RWKV-based</i>							
PointRWKV w/o vot.	96.01	95.62	93.05	96.16	92.25	10.6	2.1
PointRWKV w/ vot.	97.52	96.58	93.63	96.89	93.08	10.6	2.1

Table 1. Object classification on the ScanObjectNN and ModelNet40 datasets. We report the overall accuracy (OA, %) of ScanObjectNN on its three variants: OBJ-BG, OBJ-ONLY, and PB-T50-RS, the OA and mAcc of ModelNet40 and the overall params(M) and FLOPs(G).

For multi-scale point cloud learning, we set the scale number M to 3. For the 3-scale point clouds, we set the point numbers as $\{2048, 1024, 512\}$ with a masking ratio of 80%. We also set different k for the k -NN at different scales, which are $\{16, 8, 8\}$. In LGM, We use three iterations in our constructed graph. Data augmentation techniques involving scaling and translation are also applied. When fine-tuning the model for downstream tasks, such as classification and segmentation, we maintain the use of the AdamW optimizer but adjust the learning rate to $3e-4$ for ModelNet40 [59] and ScanObjectNN [51] classification tasks, and to $5e-4$ for the ShapeNetPart [62] segmentation task, with a weight decay of $5e-2$ and a cosine scheduler. The number of training epochs remains at 300, with a batch size adjusted to 32 for classification tasks and 16 for the segmentation task. The model architecture is consistent with the pre-training setup, with the same number of encoder and decoder layers, and input points. The augmentation strategy is adapted to fit each specific task, ensuring the model’s robustness and generalizability.

4.2. Comparison on Downstream Tasks

Real-World Object Classification on ScanObjectNN Dataset. ScanObjectNN [51], a highly challenging 3D

Method	5-way		10-way	
	10-shot ↑	20-shot ↑	10-shot ↑	20-shot ↑
DGCNN [54]	91.8 ± 3.7	93.4 ± 3.2	86.3 ± 6.2	90.9 ± 5.1
DGCNN + OcCo [53]	91.9 ± 3.3	93.9 ± 3.1	86.4 ± 5.4	91.3 ± 4.6
Transformer [64]	87.8 ± 5.2	93.3 ± 4.3	84.6 ± 5.5	89.4 ± 6.3
Transformer + OcCo [64]	94.0 ± 3.6	95.9 ± 2.3	89.4 ± 5.1	92.4 ± 4.6
Point-BERT [64]	94.6 ± 3.1	96.3 ± 2.7	91.0 ± 5.4	92.7 ± 5.1
Point-M2AE [66]	96.8 ± 1.8	98.3 ± 1.4	92.3 ± 4.5	95.0 ± 3.0
PointMamba [25]	95.0 ± 2.3	97.3 ± 1.8	91.4 ± 4.4	92.8 ± 4.0
Mamba3D [15]	96.4 ± 2.2	98.2 ± 1.2	92.4 ± 4.1	95.2 ± 2.9
PointRWKV(ours)	97.9 ± 1.2	99.2 ± 0.6	94.8 ± 2.8	96.7 ± 2.6
<i>Improvement</i>	+1.1	+0.9	+2.5	+1.5

Table 2. Few-shot classification on ModelNet40. We report the average accuracy (%) and standard deviation (%) of 10 independent experiments without voting.

dataset, encompasses approximately 15,000 objects distributed across 15 distinct categories. These objects, derived from real-world indoor environments characterized by cluttered backgrounds, contribute to the heightened complexity inherent in the task of object classification. As shown in Table 1, we conduct experiments on its three variants: OBJ-BG, OBJ-ONLY, and PB-T50-RS. After pre-training, our proposed PointRWKV consistently outper-

Method	Backbone	Cls. mIoU (%) \uparrow	Inst. mIoU (%) \uparrow	Params(M) \downarrow	FLOPs(G) \downarrow
PointNet [42]	MLP-based	80.39	83.7	3.6	4.9
PointNet++ [43]	MLP-based	81.85	85.1	1.0	4.9
PointCNN [24]	CNN-based	84.6	86.1	-	-
DGCNN [54]	CNN-based	82.3	85.2	1.3	12.4
APES [55]	MLP-based	83.67	85.8	-	-
PointMLP [31]	MLP-based	84.6	86.1	-	-
PointNeXt [45]	MLP-based	85.2 \pm 0.1	87.0 \pm 0.1	22.5	110.2
Transformer [52]	Transformer-based	83.4	85.1	27.1	15.5
PointTransformer [69]	Transformer-based	83.7	86.6	-	-
Point-BERT [64]	Transformer-based	84.1	85.6	27.1	10.6
Point-MAE [36]	Transformer-based	84.2	86.1	27.1	15.5
Point-M2AE [66]	Transformer-based	84.86	86.51	-	-
PCM [67]	Mamba-based	85.6	87.1	34.2	45.0
PointMamba [25]	Mamba-based	84.42	86.0	17.4	14.3
Mamba3D [15]	Mamba-based	84.1	85.7	21.9	9.5
PointRWKV(ours)	RWKV-based	89.87	90.26	15.2	6.5

Table 3. Part segmentation on ShapeNetPart dataset. The class mIoU and the instance mIoU are reported, with model parameters (M) and FLOPs (G).

forms transformer- and mamba-based models. Specifically, PointRWKV outperforms previous sota Mamba3D by 2.34%, 3.98% and 4.66% on three variants while reducing 37.2% parameters and 46.2% FLOPs. When compared to the transformer-based methods like Point-BERT, Point-MAE and Point-M2AE, PointRWKV demonstrates a substantial improvement, achieving 10.56%, 8.45% and 7.2% higher accuracy on the challenging PB-T50-RS subset, respectively. Even without the voting strategy [27], our PointRWKV still performs better than other methods that are tested with voting strategy.

Synthetic Object Classification on ModelNet40 Dataset.

ModelNet40 [59] is a CAD 3D object classification dataset, which includes over 12K synthetic 3D CAD models cover 40 categories in total. As shown in Table 1, we report overall accuracy (OA) and mAcc results. PointRWKV maintains its dominance with an OA of 96.89%, which is 1.79% higher than Mamba3D’s 95.1%. PointRWKV also shows a 2.89% improvement over Point-M2AE, which has an OA of 94.0%. Similarly, our PointRWKV still outperforms other methods even without the voting strategy [27]. Overall, these results highlight PointRWKV’s superiority over existing transformer- or mamba-based models, achieving multiple SoTA and demonstrating its strength across various settings.

Part Segmentation on ShapeNetPart Dataset. We conduct part segmentation on the challenging ShapeNetPart [62] dataset to predict more detailed class labels for each point within a sample. It comprises 16880 models with 16 different shape categories and 50 part labels. Experimental results on the ShapeNetPart dataset are shown in Table 3.

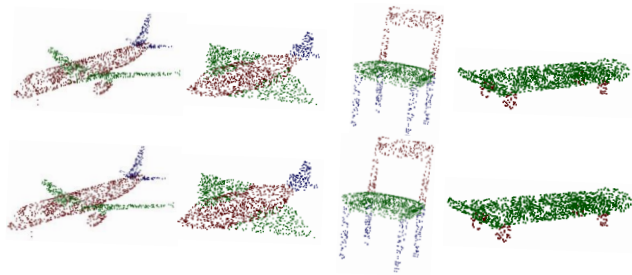


Figure 4. Part segmentation results on ShapeNetPart. Top row is ground truth and bottom row is our prediction.

We report mean IoU (mIoU) for all classes (Cls.) and all instances (Inst.). Our PointRWKV still obtains 3.16% and 4.27% improvements in terms of Inst. mIoU and Cls. mIoU while significantly reducing parameters and FLOPs. Moreover, we present qualitative results of part segmentation in Figure 4. It can be found that PointRWKV achieves highly competitive results compared to the ground truth.

Few-shot Learning. To further evaluate the performance of PointRWKV with limited fine-tuning data, we conduct experiments for few-shot classification on ModelNet40 with an n -way, m -shot setting, where n is the number of classes randomly sampled from the dataset, and m denotes the number of samples randomly drawn from each class. As shown in Table 2, we experiment with $n \in \{5, 10\}$ and $m \in \{10, 20\}$. PointRWKV surpasses previous methods by 1.1%, 0.9%, 2.5%, and 1.5%, respectively, for all four settings with much smaller deviations. This illustrates PointRWKV’s competence in learning semantic information and

Variant	OA	mAcc
base	89.6	88.3
+ BQE	90.4	89.0
+ bi-attention	91.6	90.2
+ Multi-scale	92.8	90.6
+ LGM w/o GS	93.0	91.1
+ LGM w/ GS	93.6	91.7

Table 4. Ablation of main components.

Scales	OA	mAcc
512	90.3	88.9
1024	89.6	88.3
2048	90.2	89.5
4096	89.7	88.8
512-1024-2048	92.8	91.6
1024-2048-4096	91.5	90.1

Table 5. Ablation of different point scales.

Number	OA	mAcc
0	91.2	90.5
1	92.1	91.2
2	92.4	91.4
3	92.5	91.7
4	92.3	91.5

Table 6. Ablation of different number of graph iteration.

its potent ability to transfer knowledge to downstream tasks, even with limited data.

Structural Efficiency. To fully explore the efficiency of our method, we gradually increase the sequence length to test the ability of processing the long point sequence. As shown as Figure 2, when the sequence continues to increase, we reduce the GFLOPs by $15.4\times$ and $2.1\times$ compared with the transformer-based method and the most convincing mamba-based method, achieving true linear complexity. Furthermore, as illustrated in the last two columns of Table 1 and Table 3, our PointRWKV reduces 3.1%-13.8% in parameters and 31.6%-41.7% in FLOPs when compared with transformer- and mamba-based counterparts.

4.3. Ablation Study

To investigate the effectiveness of each component and design, we conduct ablation studies on ScanObjectNN with the PB-T50-RS variant unless specified.

Analysis of Different Components. We illustrate the importance of different components of our network by adding different parts. The baseline setting is to only use single scale of 1024 points as input and remove the BQE, bidirectional attention mechanism, the LGM and graph stabilizer (GS) mechanism. As shown in Table 4, we add the shift by bidirectional quadratic expansion (BQE) function and the modified bidirectional attention mechanism, enhancing OA almost equally, respectively. We also observe that applying the hierarchical multi-scale point cloud learning and local graph-based merging can lift the performance by a large margin, which demonstrates the importance of refined feature learning. And the absence of graph stabilizer hurts the performance, which also proves the necessity of local graph adjustments.

Ablations of Different Point Scales. In Table 5, we experiment with different scales of points as input to encode the token embeddings. Apart from the original single 1024 points input, we also sample different points and combine adjacent scale to form the multi-scales embeddings. It can be observed that single-scale input fluctuates in accuracy, but multi-scale input has more outstanding final performance.

Ablations of Different Number of Graph Iteration. In local graph-based merging branch, we refine the vertex states iteratively. In Table 6, we study the impact of the number of iterations on the accuracy. The initial vertex state alone achieves the lowest accuracy since it only has a small receptive field around the vertex. As the number of iterations increases, the corresponding accuracy value also becomes higher compared to no iteration. This largely illustrates the effectiveness of the iterative graph stabilizer.

Ratio	OA	mAcc
0	87.3	86.2
0.5	91.5	90.6
0.6	91.8	90.8
0.7	92.4	91.3
0.8	92.8	91.6
0.9	92.1	91.2

Table 7. Different Masking Strategy.

Ablation of Different Masking Strategy. In Table 7, we report the results of different masking strategies during the multi-scale points processing. For different mask ratios, we find the 80% ratio performs the best to build a proper representation for hierarchical point cloud learning.

5. Conclusion

In this paper, we introduce PointRWKV, a novel RWKV-based architecture for point cloud learning. With a hierarchical architecture, PointRWKV learns to produce powerful 3D representations by encoding multi-scale point clouds. To facilitate local and global feature aggregation, we design the parallel feature merging strategy. Experimental results show that PointRWKV exhibits superior performance over transformer- and mamba-based counterparts on different point cloud learning datasets while significantly reducing parameters and FLOPs. With its linear complexity capability, we hope PointRWKV will serve as an efficient and cost-effective baseline for more 3D tasks.

Limitations and Broader Impact. The model still relies on the pre-training scheme, and more elegant methods should be designed. This study makes the initial attempt to apply RWKV in 3D point cloud learning, laying a foundation for future research.

References

- [1] Quentin Anthony, Yury Tokpanov, Paolo Glorioso, and Beren Millidge. Blackmamba: Mixture of experts for state-space models. *arXiv preprint arXiv:2402.01771*, 2024. **3**
- [2] Iro Armeni, Ozan Sener, Amir R Zamir, Helen Jiang, Ioannis Brilakis, Martin Fischer, and Silvio Savarese. 3d semantic parsing of large-scale indoor spaces. In *Proceedings of the IEEE conference on computer vision and pattern recognition*, pages 1534–1543, 2016. **12**
- [3] Matan Atzmon, Haggai Maron, and Yaron Lipman. Point convolutional neural networks by extension operators. *arXiv preprint arXiv:1803.10091*, 2018. **1, 3**
- [4] Jon L Bentley, Donald F Stanat, and E Hollins Williams Jr. The complexity of finding fixed-radius near neighbors. *Information processing letters*, 6(6):209–212, 1977. **5**
- [5] Angel X Chang, Thomas Funkhouser, Leonidas Guibas, Pat Hanrahan, Qixing Huang, Zimo Li, Silvio Savarese, Manolis Savva, Shuran Song, Hao Su, et al. Shapenet: An information-rich 3d model repository. *arXiv preprint arXiv:1512.03012*, 2015. **2, 5**
- [6] Christopher Choy, JunYoung Gwak, and Silvio Savarese. 4d spatio-temporal convnets: Minkowski convolutional neural networks. In *Proceedings of the IEEE/CVF conference on computer vision and pattern recognition*, pages 3075–3084, 2019. **3**
- [7] Xin Deng, WenYu Zhang, Qing Ding, and XinMing Zhang. Pointvector: a vector representation in point cloud analysis. In *Proceedings of the IEEE/CVF Conference on Computer Vision and Pattern Recognition*, pages 9455–9465, 2023. **3**
- [8] Jacob Devlin, Ming-Wei Chang, Kenton Lee, and Kristina Toutanova. Bert: Pre-training of deep bidirectional transformers for language understanding. *arXiv preprint arXiv:1810.04805*, 2018. **3**
- [9] Alexey Dosovitskiy, Lucas Beyer, Alexander Kolesnikov, Dirk Weissenborn, Xiaohua Zhai, Thomas Unterthiner, Mostafa Dehghani, Matthias Minderer, Georg Heigold, Sylvain Gelly, et al. An image is worth 16x16 words: Transformers for image recognition at scale. *arXiv preprint arXiv:2010.11929*, 2020. **1, 3**
- [10] Yuchen Duan, Weiyun Wang, Zhe Chen, Xizhou Zhu, Lewei Lu, Tong Lu, Yu Qiao, Hongsheng Li, Jifeng Dai, and Wenhui Wang. Vision-rwkv: Efficient and scalable visual perception with rwkv-like architectures. *arXiv preprint arXiv:2403.02308*, 2024. **3**
- [11] Daniel Y Fu, Tri Dao, Khaled K Saab, Armin W Thomas, Atri Rudra, and Christopher Ré. Hungry hungry hippos: Towards language modeling with state space models. In *ICLR*, 2022. **3**
- [12] Albert Gu and Tri Dao. Mamba: Linear-time sequence modeling with selective state spaces. *arXiv preprint arXiv:2312.00752*, 2023. **2, 3**
- [13] Meng-Hao Guo, Jun-Xiong Cai, Zheng-Ning Liu, Tai-Jiang Mu, Ralph R Martin, and Shi-Min Hu. Pct: Point cloud transformer. *Computational Visual Media*, 7:187–199, 2021. **3**
- [14] Abdullah Hamdi, Silvio Giancola, and Bernard Ghanem. Mvtn: Multi-view transformation network for 3d shape recognition. In *Proceedings of the IEEE/CVF International Conference on Computer Vision*, pages 1–11, 2021. **6, 13**
- [15] Xu Han, Yuan Tang, Zhaoxuan Wang, and Xianzhi Li. Mamba3d: Enhancing local features for 3d point cloud analysis via state space model. *arXiv preprint arXiv:2404.14966*, 2024. **2, 3, 6, 7, 13**
- [16] Ali Hatamizadeh, Yucheng Tang, Vishwesh Nath, Dong Yang, Andriy Myronenko, Bennett Landman, Holger R Roth, and Daguang Xu. Unetr: Transformers for 3d medical image segmentation. In *Proceedings of the IEEE/CVF winter conference on applications of computer vision*, pages 574–584, 2022. **3**
- [17] Haoyang He, Yuhu Bai, Jiangning Zhang, Qingdong He, Hongxu Chen, Zhenye Gan, Chengjie Wang, Xiangtai Li, Guanzhong Tian, and Lei Xie. Mambaad: Exploring state space models for multi-class unsupervised anomaly detection. *arXiv preprint arXiv:2404.06564*, 2024. **3**
- [18] Qingdong He, Zhengning Wang, Hao Zeng, Yi Zeng, and Yijun Liu. Svga-net: Sparse voxel-graph attention network for 3d object detection from point clouds. In *Proceedings of the AAAI Conference on Artificial Intelligence*, pages 870–878, 2022. **3**
- [19] Tianxin Huang, Jiangning Zhang, Jun Chen, Zhonggan Ding, Ying Tai, Zhenyu Zhang, Chengjie Wang, and Yong Liu. 3qnet: 3d point cloud geometry quantization compression network. *ACM TOG*, 2022. **3**
- [20] Tianxin Huang, Hao Zou, Jinhao Cui, Jiangning Zhang, Xue-meng Yang, Lin Li, and Yong Liu. Adaptive recurrent forward network for dense point cloud completion. *TMM*, 2022.
- [21] Tianxin Huang, Zhonggan Ding, Jiangning Zhang, Ying Tai, Zhenyu Zhang, Mingang Chen, Chengjie Wang, and Yong Liu. Learning to measure the point cloud reconstruction loss in a representation space. In *CVPR*, 2023. **3**
- [22] Artem Komarichev, Zichun Zhong, and Jing Hua. A-cnn: Annularly convolutional neural networks on point clouds. In *Proceedings of the IEEE/CVF conference on computer vision and pattern recognition*, pages 7421–7430, 2019. **1, 3**
- [23] Loic Landrieu and Martin Simonovsky. Large-scale point cloud semantic segmentation with superpoint graphs. In *Proceedings of the IEEE conference on computer vision and pattern recognition*, pages 4558–4567, 2018. **3**
- [24] Yangyan Li, Rui Bu, Mingchao Sun, Wei Wu, Xinhan Di, and Baoquan Chen. Pointcnn: Convolution on x-transformed points. *Advances in neural information processing systems*, 31, 2018. **1, 3, 6, 7, 13**
- [25] Dingkan Liang, Xin Zhou, Xinyu Wang, Xingkui Zhu, Wei Xu, Zhikang Zou, Xiaoqing Ye, and Xiang Bai. Pointmamba: A simple state space model for point cloud analysis. *arXiv preprint arXiv:2402.10739*, 2024. **1, 2, 3, 6, 7, 13**
- [26] Jiuming Liu, Ruiji Yu, Yian Wang, Yu Zheng, Tianchen Deng, Weicai Ye, and Hesheng Wang. Point mamba:

- A novel point cloud backbone based on state space model with octree-based ordering strategy. *arXiv preprint arXiv:2403.06467*, 2024. 2, 3
- [27] Yongcheng Liu, Bin Fan, Shiming Xiang, and Chunhong Pan. Relation-shape convolutional neural network for point cloud analysis. In *Proceedings of the IEEE/CVF conference on computer vision and pattern recognition*, pages 8895–8904, 2019. 7
- [28] Yue Liu, Yunjie Tian, Yuzhong Zhao, Hongtian Yu, Lingxi Xie, Yaowei Wang, Qixiang Ye, and Yunfan Liu. Vmamba: Visual state space model. *arXiv preprint arXiv:2401.10166*, 2024. 2, 3
- [29] Ze Liu, Yutong Lin, Yue Cao, Han Hu, Yixuan Wei, Zheng Zhang, Stephen Lin, and Baining Guo. Swin transformer: Hierarchical vision transformer using shifted windows. In *Proceedings of the IEEE/CVF international conference on computer vision*, pages 10012–10022, 2021. 1, 3
- [30] Ilya Loshchilov and Frank Hutter. Decoupled weight decay regularization. *arXiv preprint arXiv:1711.05101*, 2017. 5
- [31] Xu Ma, Can Qin, Haoxuan You, Haoxi Ran, and Yun Fu. Rethinking network design and local geometry in point cloud: A simple residual mlp framework. *arXiv preprint arXiv:2202.07123*, 2022. 1, 3, 6, 7, 13
- [32] Jiageng Mao, Yujing Xue, Minzhe Niu, Haoyue Bai, Jia-shi Feng, Xiaodan Liang, Hang Xu, and Chunjing Xu. Voxel transformer for 3d object detection. In *Proceedings of the IEEE/CVF international conference on computer vision*, pages 3164–3173, 2021. 3
- [33] Jiageng Mao, Shaoshuai Shi, Xiaogang Wang, and Hongsheng Li. 3d object detection for autonomous driving: A review and new outlooks. *arXiv preprint arXiv:2206.09474*, 1, 2022. 1
- [34] Harsh Mehta, Ankit Gupta, Ashok Cutkosky, and Behnam Neyshabur. Long range language modeling via gated state spaces. In *ICLR*, 2022. 3
- [35] Ishan Misra, Rohit Girdhar, and Armand Joulin. An end-to-end transformer model for 3d object detection. In *Proceedings of the IEEE/CVF International Conference on Computer Vision*, pages 2906–2917, 2021. 3
- [36] Yatian Pang, Wenxiao Wang, Francis EH Tay, Wei Liu, Yonghong Tian, and Li Yuan. Masked autoencoders for point cloud self-supervised learning. In *European conference on computer vision*, pages 604–621. Springer, 2022. 1, 3, 5, 6, 7
- [37] Chunghyun Park, Yoonwoo Jeong, Minsu Cho, and Jaesik Park. Fast point transformer. In *Proceedings of the IEEE/CVF Conference on Computer Vision and Pattern Recognition*, pages 16949–16958, 2022. 3
- [38] Youngmin Park, Vincent Lepetit, and Woontack Woo. Multiple 3d object tracking for augmented reality. In *2008 7th IEEE/ACM International Symposium on Mixed and Augmented Reality*, pages 117–120. IEEE, 2008. 1
- [39] Bo Peng, Eric Alcaide, Quentin Anthony, Alon Albalak, Samuel Arcadinho, Huanqi Cao, Xin Cheng, Michael Chung, Matteo Grella, Kranthi Kiran GV, et al. Rwkv: Reinventing rnns for the transformer era. *arXiv preprint arXiv:2305.13048*, 2023. 2, 3
- [40] Bo Peng, Daniel Goldstein, Quentin Anthony, Alon Albalak, Eric Alcaide, Stella Biderman, Eugene Cheah, Teddy Ferdinan, Haowen Hou, Przemysław Kazienko, et al. Eagle and finch: Rwkv with matrix-valued states and dynamic recurrence. *arXiv preprint arXiv:2404.05892*, 2024. 3
- [41] Maciej Pióro, Kamil Ciebiera, Krystian Król, Jan Ludziejewski, and Sebastian Jaszczur. Moe-mamba: Efficient selective state space models with mixture of experts. *arXiv preprint arXiv:2401.04081*, 2024. 3
- [42] Charles R Qi, Hao Su, Kaichun Mo, and Leonidas J Guibas. Pointnet: Deep learning on point sets for 3d classification and segmentation. In *Proceedings of the IEEE conference on computer vision and pattern recognition*, pages 652–660, 2017. 1, 3, 6, 7, 13
- [43] Charles Ruizhongtai Qi, Li Yi, Hao Su, and Leonidas J Guibas. Pointnet++: Deep hierarchical feature learning on point sets in a metric space. *Advances in neural information processing systems*, 30, 2017. 1, 3, 6, 7, 13
- [44] Zekun Qi, Runpei Dong, Guofan Fan, Zheng Ge, Xiangyu Zhang, Kaisheng Ma, and Li Yi. Contrast with reconstruct: Contrastive 3d representation learning guided by generative pretraining. In *International Conference on Machine Learning*, pages 28223–28243. PMLR, 2023. 1
- [45] Guocheng Qian, Yuchen Li, Houwen Peng, Jinjie Mai, Hasan Hammoud, Mohamed Elhoseiny, and Bernard Ghanem. Pointnext: Revisiting pointnet++ with improved training and scaling strategies. *Advances in Neural Information Processing Systems*, 35:23192–23204, 2022. 1, 3, 6, 7, 13
- [46] Alec Radford, Karthik Narasimhan, Tim Salimans, Ilya Sutskever, et al. Improving language understanding by generative pre-training. 2018. 3
- [47] Olaf Ronneberger, Philipp Fischer, and Thomas Brox. U-net: Convolutional networks for biomedical image segmentation. In *Medical image computing and computer-assisted intervention—MICCAI 2015: 18th international conference, Munich, Germany, October 5–9, 2015, proceedings, part III 18*, pages 234–241. Springer, 2015. 2
- [48] Nur Muhammad Mahi Shafullah, Chris Paxton, Lerrel Pinto, Soumith Chintala, and Arthur Szlam. Clip-fields: Weakly supervised semantic fields for robotic memory. *arXiv preprint arXiv:2210.05663*, 2022. 1
- [49] Jimmy TH Smith, Andrew Warrington, and Scott W Linderman. Simplified state space layers for sequence modeling. In *ICLR*, 2022. 3
- [50] Hugues Thomas, Charles R Qi, Jean-Emmanuel Deschaud, Beatriz Marcotegui, François Goulette, and Leonidas J Guibas. Kpconv: Flexible and deformable convolution for point clouds. In *Proceedings of the IEEE/CVF international conference on computer vision*, pages 6411–6420, 2019. 1, 3
- [51] Mikaela Angelina Uy, Quang-Hieu Pham, Binh-Son Hua, Thanh Nguyen, and Sai-Kit Yeung. Revisiting point cloud classification: A new benchmark dataset and classification model on real-world data. In *Proceedings of the IEEE/CVF international conference on computer vision*, pages 1588–1597, 2019. 2, 6

- [52] Ashish Vaswani, Noam Shazeer, Niki Parmar, Jakob Uszkoreit, Llion Jones, Aidan N Gomez, Łukasz Kaiser, and Illia Polosukhin. Attention is all you need. *Advances in neural information processing systems*, 30, 2017. **3, 6, 7**
- [53] Hanchen Wang, Qi Liu, Xiangyu Yue, Joan Lasenby, and Matt J Kusner. Unsupervised point cloud pre-training via occlusion completion. In *Proceedings of the IEEE/CVF international conference on computer vision*, pages 9782–9792, 2021. **6**
- [54] Yue Wang, Yongbin Sun, Ziwei Liu, Sanjay E Sarma, Michael M Bronstein, and Justin M Solomon. Dynamic graph cnn for learning on point clouds. *ACM Transactions on Graphics (tog)*, 38(5):1–12, 2019. **1, 3, 6, 7, 13**
- [55] Chengzhi Wu, Junwei Zheng, Julius Pfommer, and Jürgen Beyerer. Attention-based point cloud edge sampling. In *Proceedings of the IEEE/CVF Conference on Computer Vision and Pattern Recognition*, pages 5333–5343, 2023. **7**
- [56] Wenxuan Wu, Zhongang Qi, and Li Fuxin. Pointconv: Deep convolutional networks on 3d point clouds. In *Proceedings of the IEEE/CVF Conference on computer vision and pattern recognition*, pages 9621–9630, 2019. **1, 3**
- [57] Xiaoyang Wu, Yixing Lao, Li Jiang, Xihui Liu, and Hengshuang Zhao. Point transformer v2: Grouped vector attention and partition-based pooling. *Advances in Neural Information Processing Systems*, 35:33330–33342, 2022. **1, 3**
- [58] Xiaoyang Wu, Li Jiang, Peng-Shuai Wang, Zhijian Liu, Xihui Liu, Yu Qiao, Wanli Ouyang, Tong He, and Hengshuang Zhao. Point transformer v3: Simpler, faster, stronger. *arXiv preprint arXiv:2312.10035*, 2023. **1, 3**
- [59] Zhirong Wu, Shuran Song, Aditya Khosla, Fisher Yu, Linguang Zhang, Xiaoou Tang, and Jianxiong Xiao. 3d shapenets: A deep representation for volumetric shapes. In *Proceedings of the IEEE conference on computer vision and pattern recognition*, pages 1912–1920, 2015. **2, 6, 7**
- [60] Yijun Yang, Zhaohu Xing, and Lei Zhu. Vivim: a video vision mamba for medical video object segmentation. *arXiv preprint arXiv:2401.14168*, 2024. **3**
- [61] Zhiwen Yang, Hui Zhang, Dan Zhao, Bingzheng Wei, and Yan Xu. Restore-rwkv: Efficient and effective medical image restoration with rwkv, 2024. **3**
- [62] Li Yi, Vladimir G Kim, Duygu Ceylan, I-Chao Shen, Mengyan Yan, Hao Su, Cewu Lu, Qixing Huang, Alla Sheffer, and Leonidas Guibas. A scalable active framework for region annotation in 3d shape collections. *ACM Transactions on Graphics (ToG)*, 35(6):1–12, 2016. **2, 6, 7**
- [63] Xumin Yu, Yongming Rao, Ziyi Wang, Zuyan Liu, Jiwen Lu, and Jie Zhou. Pointtr: Diverse point cloud completion with geometry-aware transformers. In *Proceedings of the IEEE/CVF international conference on computer vision*, pages 12498–12507, 2021. **3**
- [64] Xumin Yu, Lulu Tang, Yongming Rao, Tiejun Huang, Jie Zhou, and Jiwen Lu. Point-bert: Pre-training 3d point cloud transformers with masked point modeling. In *Proceedings of the IEEE/CVF conference on computer vision and pattern recognition*, pages 19313–19322, 2022. **1, 3, 6, 7**
- [65] Haobo Yuan, Xiangtai Li, Lu Qi, Tao Zhang, Ming-Hsuan Yang, Shuicheng Yan, and Chen Change Loy. Mamba or rwkv: Exploring high-quality and high-efficiency segment anything model. *arXiv preprint arXiv:2406.19369*, 2024. **3**
- [66] Renrui Zhang, Ziyu Guo, Peng Gao, Rongyao Fang, Bin Zhao, Dong Wang, Yu Qiao, and Hongsheng Li. Point-m2ae: multi-scale masked autoencoders for hierarchical point cloud pre-training. *Advances in neural information processing systems*, 35:27061–27074, 2022. **1, 3, 6, 7**
- [67] Tao Zhang, Xiangtai Li, Haobo Yuan, Shunping Ji, and Shuicheng Yan. Point cloud mamba: Point cloud learning via state space model. *arXiv preprint arXiv:2403.00762*, 2024. **2, 3, 6, 7, 13**
- [68] Hengshuang Zhao, Li Jiang, Chi-Wing Fu, and Jiaya Jia. Pointweb: Enhancing local neighborhood features for point cloud processing. In *Proceedings of the IEEE/CVF conference on computer vision and pattern recognition*, pages 5565–5573, 2019. **3**
- [69] Hengshuang Zhao, Li Jiang, Jiaya Jia, Philip HS Torr, and Vladlen Koltun. Point transformer. In *Proceedings of the IEEE/CVF international conference on computer vision*, pages 16259–16268, 2021. **1, 3, 6, 7, 13**
- [70] Lianghui Zhu, Bencheng Liao, Qian Zhang, Xinlong Wang, Wenyu Liu, and Xinggang Wang. Vision mamba: Efficient visual representation learning with bidirectional state space model. *arXiv preprint arXiv:2401.09417*, 2024. **2**

PointRWKV: Efficient RWKV-Like Model for Hierarchical Point Cloud Learning

Supplementary Material

The supplementary material presents the following sections to strengthen the main manuscript:

- Results of training from scratch.
- Semantic segmentation on S3DIS dataset.
- More qualitative visualization results on ShapeNetPart.

A1. Results of Training From Scratch

To further demonstrate the effectiveness of our proposed PointRWKV, we also report the results for models trained from scratch. It is noted that compared with pre-training, many methods does not report the results of training from scratch. As shown in Table A1, we conduct experiments on ScanObjectNN and ModelNet40 Dataset. Compared to previous methods, PointRWKV obtains 0.51%-2.9% overall accuracy performance gains across different variants among different datasets. When without voting strategy, PointRWKV can still outperform other methods.

A2. Semantic Segmentation on S3DIS Dataset

S3DIS [2] dataset consists of 271 rooms in six areas from three different buildings. Each point in the scan is assigned a semantic label from 13 categories. we evaluate on Area 5 as shown in Table A2. The results further demonstrate the superiority of our method over transformer- and mamba-based counterpart.

A3. More Qualitative Visualization on ShapeNetPart

In Figure A1, we illustrate more Visualizations which further shows that PointRWKV achieves highly competitive results to the ground truth.

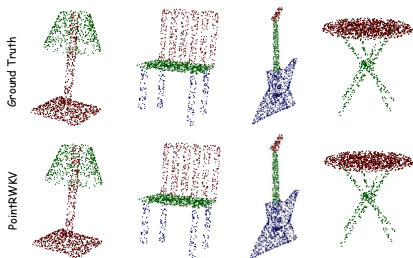


Figure A1. Qualitative results of part segmentation results on ShapeNetPart. Top row is ground truth and bottom row is our prediction.

Method	ScanObjectNN			ModelNet40		Params(M) ↓	FLOPs(G) ↓
	OBJ-BG ↑	OBJ-ONLY ↑	PB-T50-RS ↑	OA (%) ↑	mAcc (%) ↑		
<i>MLP/CNN-based</i>							
PointNet [42]	73.3	79.2	68.0	89.2	86.2	3.5	0.5
PointNet++ [43]	82.3	84.3	77.9	90.7	-	1.5	1.7
PointCNN [24]	86.1	85.5	78.5	92.2	88.1	0.6	0.9
DGCNN [54]	82.8	86.2	78.1	92.9	-	1.8	2.4
MVTN [14]	92.6	92.3	82.8	93.8	-	11.2	43.7
PointMLP [31]	-	-	85.4±0.3	94.5	91.4	12.6	31.4
PointNeXt [45]	-	-	87.7±0.4	93.2±0.1	90.8±0.2	1.4	1.6
<i>Transformer-based</i>							
PointTransformer [69]	-	-	-	93.7	90.6	22.1	4.8
<i>Mamba-based</i>							
PCM [67]	-	-	88.10±0.3	93.4±0.2	-	34.2	45.0
PointMamba [25]	88.30	87.78	82.48	92.4	-	12.3	3.6
Mamba3D [15]	94.49	92.43	92.64	94.1	-	16.9	3.9
<i>RWKV-based</i>							
PointRWKV w/o vot.	95.22	94.28	92.88	94.66	91.35	10.6	2.1
PointRWKV w/ vot.	96.53	95.33	93.15	95.36	92.48	10.6	2.1

Table A1. Object classification on the ScanObjectNN and ModelNet40 datasets of training from scratch. We report the overall accuracy (OA, %) of ScanObjectNN on its three variants: OBJ-BG, OBJ-ONLY, and PB-T50-RS, the OA and mAcc of ModelNet40 and the overall params(M) and FLOPs(G).

Method	OA	mAcc	mIoU	ceiling	floor	wall	beam	column	window	door	table	chair	sofa	bookcase	board	clutter
PointNet [42]	-	49.0	41.1	88.8	97.3	69.8	0.1	3.9	46.3	10.8	59.0	52.6	5.9	40.3	26.4	33.2
PointCNN [24]	85.9	63.9	57.3	92.3	98.2	79.4	0.0	17.6	22.8	62.1	74.4	80.6	31.7	66.7	62.1	56.7
PointNeXt-S [45]	87.9	-	63.4	-	-	-	-	-	-	-	-	-	-	-	-	-
PointCloudMamba [67]	88.2	71.0	63.4	93.3	96.7	80.6	0.1	35.9	57.7	60.0	74.0	87.6	50.1	69.4	63.5	55.9
PointRWKV(ours)	92.3	76.8	70.5	94.2	98.3	86.5	0.0	38.6	64.5	76.2	88.2	89.3	65.2	75.6	78.2	61.3

Table A2. Semantic segmentation results on S3DIS dataset.